



ORIGINAL RESEARCH ARTICLE

The Effect of Detonation Frequency on the Linear Reciprocating Wear Behavior of Detonation Sprayed Ni-20%Cr Coatings at Elevated Temperatures

Rahul Prasad, N. Purushotham, G.V. Preetham Kumar, P. Suresh Babu, G. Sivakumar, and B. Rajasekaran

Submitted: 23 December 2023 / Revised: 13 May 2024 / Accepted: 18 June 2024

The study explores the impact of detonation frequency (3 and 6 Hz) on the temperature-dependent linear reciprocating wear behavior of Ni-20%Cr coatings deposited by detonation spraying on a nickel-based superalloy (IN718). Dry sliding experiments were carried out at both ambient (25 °C) and high (420 °C) temperatures, using an alumina (Al₂O₃) ball as the counter material and different loads (5, 10, and 20 N). HV_{0.2} microhardness indentations were used to test material hardness variations attributed to heat exposure. X-ray diffraction (XRD), Raman spectroscopy, and field emission scanning electron microscopy with energy-dispersive spectroscopy (FESEM with EDS) were used to investigate the wear characteristics and mechanisms. Furthermore, surface roughness and profiles of worn surfaces (including track depth, breadth, and wear volume) enabled the calculation of wear rates using confocal optical 3D profilometry. The results showed the 6 Hz Ni-20%Cr coating showed better wear resistance than the 3 Hz coating. However, a higher wear rate and low friction coefficient at 420 °C were observed due to partial oxide particles, which were insufficient to restrict direct ball-to-metal contact. The research delves into wear maps, tribolayer formation, wear mechanisms, and sub-mechanisms.

Keywords counter material, linear reciprocating, residual stress, spray frequency, worn surface

1. Introduction

Inconel 718 (IN718) is one of the most widely preferred nickel-based superalloys due to its higher yield strength at room temperature and high-temperature range than other alloys (Ref 1). Due to its excellent mechanical characteristics at high temperatures, it is used in various industries, including aerospace, oil and gas, gas turbine, and military (Ref 2, 3). However, IN718 often exhibits poor resistance to hot corrosion environments, leading to component fatigue, wear, and potential failure (Ref 4). A study on various materials, including cobalt-based alloys, iron-based alloys, and Inconel superalloys, has discovered that cobalt- and iron-based alloys have superior wear resistance at room temperature. The interface oxide of cobalt (Co)- and iron (Fe)-based superalloys effectively enhances their wear resistance (Ref 5). Reducing friction and minimizing wear is crucial for global energy savings (Ref 6).

Thermal spray coating prevents wear and material loss, ensuring reliable protection against corrosion, oxidation, and

wear while maintaining thermal efficiency in various applications (Ref 7-9). Detonation spray coating (DSC) offers good adhesive bonding, lower porosity, denser microstructure, and compressive residual stresses among the thermal spray techniques (Ref 10-12).

Gas turbine parts must be effectively worn prevention for high-temperature applications, such as oil-free journal bearings running at 500 °C (Ref 13). More instances of gas turbine parts contacting each other slidingly at high temperatures exist. Plasma spray coating with unique powder mixtures combining NiCr, Cr₂O₃ hard phase, and solid lubricants provides the protective coatings recommended for such applications (Ref 13, 14). In high-temperature conditions, oxides of various types have been used as additives to enhance Ni-based composites' friction and wear properties. (Ref 15-17). These oxides can act as lubricants or strengthening agents, influencing the mechanical and wear characteristics of Ni-based composite coatings at high temperatures while also ensuring stability in severe conditions (Ref 18-20). However, there are insufficient studies on whether nickel-based coatings can withstand friction and wear across a wide temperature range.

Observations at average/typical temperatures have indicated simultaneous abrasion, plastic deformation, and surface fatigue in frictional contacts (Ref 7). However, the working temperature is insufficient to properly grind the worn debris, resulting in substantial wear and severe abrading of the three bodies due to subsequent oxidation (Ref 21). The wear shifts from extreme to moderate when the temperature reaches a certain level. This shift is related to the development of a significant oxide film, known as "glaze," due to tribo-sintering, which involves the formation of an oxide film from oxide debris (Ref 22).

The study reveals that as temperature increases, the unidirectional dry sliding wear behavior of Ni-20%Cr coatings

Rahul Prasad, N. Purushotham, G.V. Preetham Kumar, and B. Rajasekaran, Department of Metallurgical and Materials Engineering, National Institute of Technology, Karnataka (NITK), 575025 Surathkal, India; P. Suresh Babu and G. Sivakumar, International Advanced Research Center For Powder Metallurgy And New Materials, Hyderabad 500 005, India. Contact e-mail: b.raajasekaran@nitk.edu.in.

decreases due to the formation of composite layers. Besides, the temperature-dependent material parameters that can affect the linear reciprocating wear resistance of Ni-20%Cr coatings at high temperatures include hardness, coefficient of thermal expansion (CTE), oxidation resistance, grain size, microstructure, and phase transformations (Ref 23). The linear reciprocating dry sliding wear test assesses materials wear resistance and behavior in a dry sliding, making it suitable for systems with linear sliding contacts like piston rings, cylinder liners, and valve components (Ref 24, 25).

At high temperatures, the Ni-20%Cr coating exhibits a higher coefficient of thermal expansion and is closer to the base material, resulting in low tensile residual stress (Ref 23). Peening stress is the sole contributing factor to compressive residual stress, dominated by high spray frequency. Lower spray frequency leads to a lower peening effect, affecting the final residual stress on thermal spray coating (Ref 26, 27).

This study compares the effect of spray frequency (3 and 6 Hz) on dry sliding linear reciprocating wear behavior of DSC sprayed Ni-20%Cr coatings at elevated temperatures (25 and 420 °C) with different loads (5, 10, and 20 N). The inquiry also explores the measures of residual stress through the XRD. Additionally, the study investigates the wear maps and mechanisms at different temperatures using surface characterization techniques.

2. Experimentation

2.1 Feedstock Material and Coating Deposition Technique

The nickel-based superalloy (IN718) was used as the base material, and nichrome powder (Ni-20%Cr, Amperit-251, Germany) was used as a feedstock for coating deposition. The substrate was grit-blasted before detonation spray coating to ensure good bonding at the interface. The indigenous coating deposition system was implemented at ARCI in Hyderabad, India. The optimized process parameters are mentioned in Table 1.

2.2 Evaluation of Mechanical Properties and Tribological Behavior

A microhardness test was conducted on 3 and 6 Hz Ni-20%Cr-coated samples using a Vickers microhardness tester (HVM-G-20ST version 1.03, SHIMADZU). After polishing, a smooth surface was achieved, and diamond-shaped indentations were performed on the well-polished cross section. A

200 g load was used, with a 15-second dwell time, and at least 15 indentations were performed for each sample.

A dry sliding linear reciprocating wear test was performed on Ni-20%Cr-coated samples at different frequencies (3 and 6 Hz). Before the test, the surfaces of the coated sample were mechanically polished to $0.27 \pm 0.04 \mu\text{m}$ to prevent errors in wear test results. Wear experiments consisting of linear reciprocating motion were conducted in ambient air using a ball-on-flat tribometer setup (TRB³, Anton Paar, Austria). Test parameters were established according to ASTM G-133 standards using an Al₂O₃ ball with a hardness of $(700 \pm 20 \text{ HV})$ as shown in Table 2. Each condition was tested at least three times to ensure precision and consistency. The wear coefficient was calculated using the expression mentioned in (Ref 28).

2.3 Surface Characterizations of Coatings

The x-ray diffraction (XRD) was performed using Malvern PANalytical 3rd generation Empyrean XRD equipment (Netherlands) to characterize coated samples. During the XRD test, Cu-K α wavelength (λ) was 1.54 Å, scan step size was 0.026, and the diffraction angle was set at 30-90°. A $\sin^2\psi$ method with the tilt angles (ψ) as -45° , -39° , -33° , -26° , -18° , 0° , 45° , 39° , 33° , 26° , 18° , and 0° was used for stress estimation. The total run time for each sample was 5 h and 30 min. After wear tests at room and high temperatures, the surface of both samples was examined using XRD to check the formation of any oxide layers. X'Pert HighScore Plus software was used to identify the phases of the diffraction peaks.

Microstructural analysis of coatings was examined using a FESEM (7610F PLUS, Jeol, Japan) with secondary (SE) and backscattered electrons (BSE) detectors. The elemental mapping and composition with percentage (%) were evaluated using FESEM-EDS microanalysis and employed to identify the wear maps and wear mechanisms of the coating and counter material post-wear under different conditions.

Following wear tests at ambient and high temperatures, Raman spectroscopy (Compact Raman Spectrometer, Renishaw Centrus 2R4P63, UK) was used to evaluate and identify the oxide on the worn surface of the wear scar for 3 and 6 Hz samples. Surface roughness and worn-out surface profiles like wear scar depth, width, and wear volume enabled calculating the wear rate with a confocal optical 3D profilometer (NANOVEA, ST-400, USA). Each condition was tested at least three times to assure accuracy and consistency.

Table 1 Optimized process parameters for coating deposition

Coating parameters of DSC	
Carrier gas (N ₂) pressure, bar	1
Spray frequency (Hz)	3 and 6
(Oxygen) flow rate (SLPM)	38
(Acetylene) flow rate (SLPM)	31
Built per pass (μm)	15 – 20
Standoff distance (mm)	165

Table 2 Parameters for linear reciprocating dry sliding wear test

Linear reciprocating wear test parameters	
Stroke length (mm)	4
Loads (N)	5, 10 & 20
Total sliding distance (m)	100
Frequency (Hz)	5
Ball diameter (mm)	6
Test temperature (°C)	(25 and 420) \pm 10
Stabilization period at high temperature (hr)	1
Total run time (Min)	42

3. Results and Discussion

3.1 As-Deposited Characterizations

3.1.1 Microstructural Characterization. Figure 1 shows the 3D profilometer and FESEM images of Ni-20%Cr coatings. Figure 1(b) and (e) shows the surface morphology of Ni-20%Cr coating with different frequencies. It exhibits many unmelted, semi-melted, and fully melted particles entrapped in the coating surface, showing high surface roughness in Fig. 1(a) and (d). 6 Hz sample has lower surface roughness than 3 Hz due to spray frequency variation. In contrast, higher frequency promotes particle flattening and reduces roughness (Ref 29). Figure 1(c) and (f) presents a cross section of the coatings with low porosity, and the excellent adhesion at the interface and resistance to spallation confirm a uniform, lamellar structure with the desired thickness as given in Table 3. Porosity was found at the interface of coating and the IN718 substrates due to mismatches in the thermophysical characteristics of the feedstock material and the substrates and unmelted particles trapped at the interface.

The 6 Hz coating exhibits lower porosity, indicating a denser coating at higher frequencies. This is due to increased powder particles' kinetic energy and velocity, resulting in better flattening and interlocking on the substrate (Ref 30). Higher deposition efficiency reduces gaps and voids, increasing coating density (Ref 31).

Figure 2 depicts an EDS investigation of coating at various frequencies. It demonstrates that nickel (Ni), chromium (Cr), and oxygen (O) elemental maps are all well matched. This basic mapping analysis indicates that the deposited coating is almost identical to the 80Ni-20Cr feedstock material. Furthermore, it suggests that layers are formed consistently with no visible segregation throughout the coating deposition process.

Figure 3 displays the stack and indexing of an as-deposited Ni-20%Cr coating with 3 and 6 Hz frequencies. It has highly narrow and strongly diffracted peaks. It was noticed that in both coatings, all diffracted peaks had the crystalline γ -Ni(Cr) (ICDD File number: 01-071-7597) phase with face-centered cube (FCC) solid solution crystal structure, and there were no other peaks on the coating.

3.1.2 Residual Stress Analysis. The residual stress was evaluated on the surface of the coating, with quantitative data in Table 4 and a trend line shown in Fig. 4. As frequency increased, the stress decreased numerically. The 3 Hz sample had minimal tensile stress, while the 6 Hz sample had the highest compressive stress. This difference could be attributed to the processing conditions, such as spray frequency. As coating thickness increases, residual stress typically transforms from tensile to compressive, reaching a certain point (Ref 32, 33).

3.2 Evaluation of Microhardness of Coatings

Table 5 shows the microhardness of the Ni-20%Cr coatings with temperatures and spray frequencies. The 6 Hz coating had higher hardness than the 3 Hz at ambient temperature. This difference is due to densification and stronger bonding of splats at higher spray frequencies. Tensile residual stress decreases the hardness of samples, while high-compressive residual stress material exhibits a high hardness value (Ref 34, 35). The varying state of residual stress on both coating surfaces contributes to higher hardness for the 6 Hz coating and lower hardness for the 3 Hz coating.

The Ni-20%Cr coating showed high microhardness at 25 °C due to the fast cooling rate, strain hardening, and metallic and partial oxide phases (Ref 36). Nonetheless, there was a decrease in microhardness at 420 °C due to thermal softening and annealing. This resulted in more visible grain development,

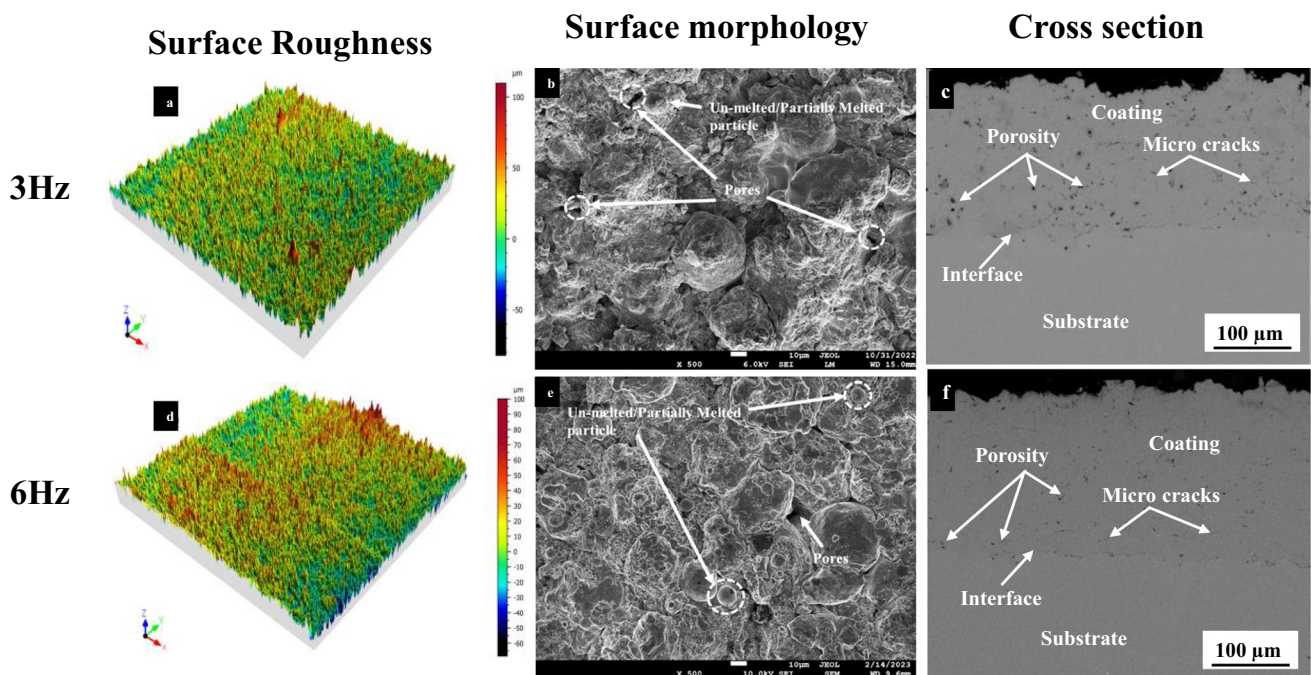


Fig. 1 Micrographs of as-sprayed Ni-20%Cr coatings: (a and d) surface roughness by 3D profilometer, (b and e) surface morphology, (c and f) cross section

Table 3 Thickness, porosity, and surface roughness of Ni-20%Cr coatings

Samples	Spray frequency, Hz	Thickness of coating, μm	Porosity, %	Surface roughness S_a , μm
Ni-20%Cr	3	266 ± 12	2.18 ± 0.3	10.3 ± 0.7
	6	324 ± 12	1.28 ± 0.1	7.6 ± 0.2

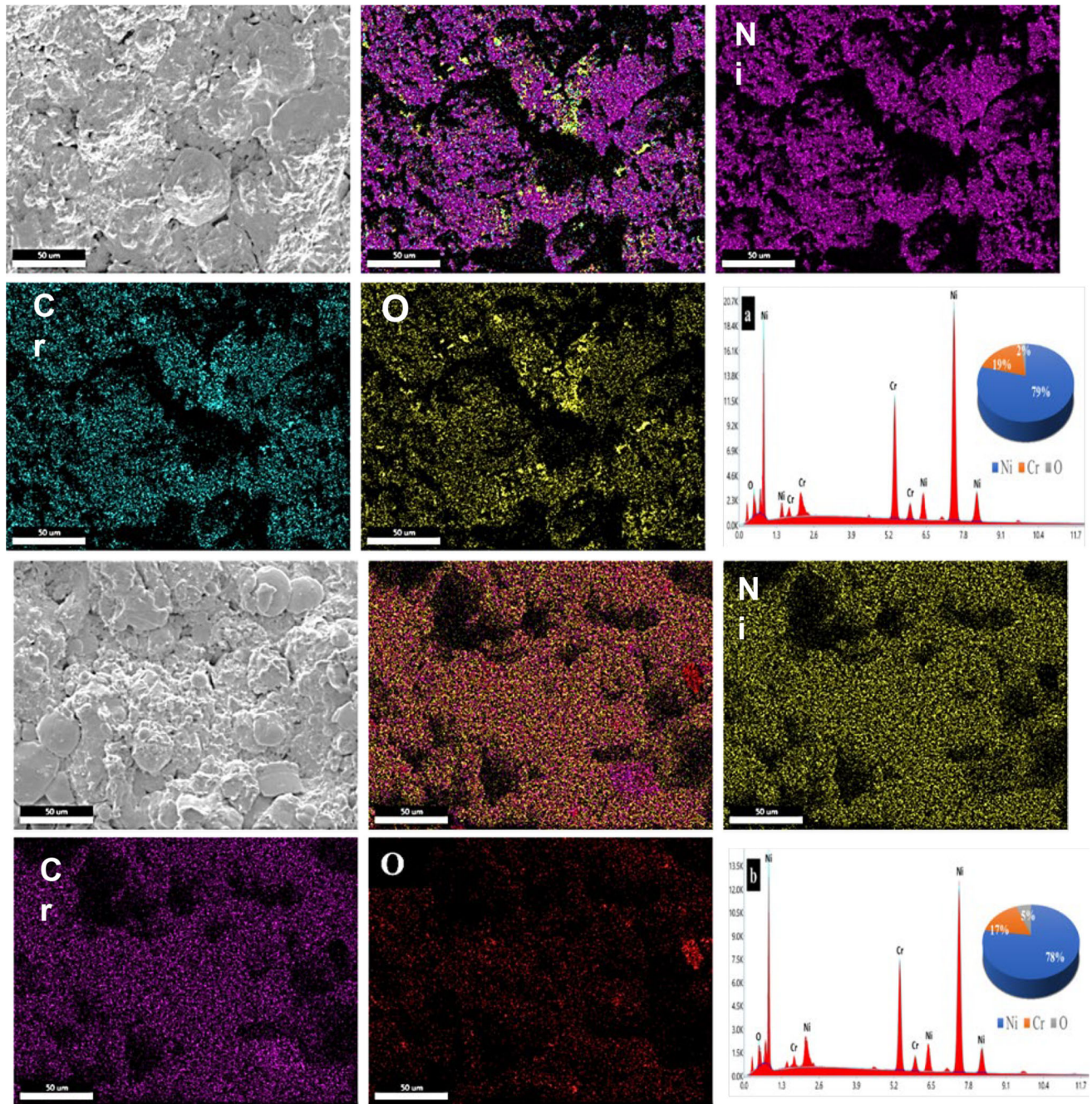


Fig. 2 EDS elemental analysis of as-sprayed coating at different frequencies: (a) 3 Hz and (b) 6 Hz

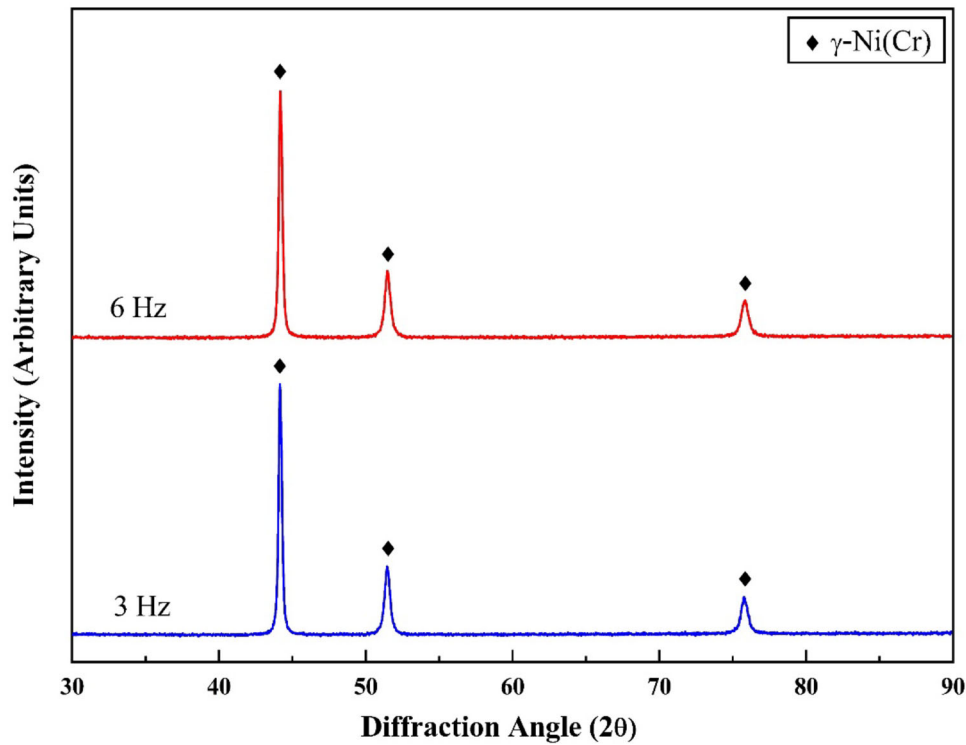


Fig. 3 XRD analysis of Ni-20%Cr coating with different spray frequencies

Table 4 Quantitative residual stress values of as-deposited Ni-20%Cr coating

Sample	Spray frequency, Hz	Residual stress, MPa
Ni-20%Cr	3	9.8 ± 3.0
	6	-14.6 ± 2.9

reduced shear strength, simpler plastic deformation, and reduced surface residual stresses (Ref 37) (Table 6).

3.3 Linear Reciprocating Wear Behavior

Figure 5 shows the coefficient of friction (CoF) vs. sliding distance (m) trend for 3 and 6 Hz samples at 25 and 420 °C under different loads (5, 10, and 20 N). At room temperature, the 6 Hz coating has a higher CoF than the 3 Hz coating. This is because the 6 Hz coating has a higher oxide concentration, making it less capable of bearing weight and creating more friction between the coating and counter material. This trend also occurs at high temperatures, possibly due to the high oxide content in the Ni-20%Cr coating, making it prone to spalling during high-temperature sliding. Both coatings demonstrate increased deformation, cracking, interfacial shear stress, and CoF as loads increase (Ref 38).

CoF values for wear tests at 420 °C were lower than at ambient temperature. At higher temperatures, the coating material undergoes thermal softening, which reduces interfacial shear stress (Ref 39). The formation of oxide layers on sliding surfaces can also reduce CoF, as oxide particles/surfaces act as solid lubricants. It reduces the adhesion phenomenon and resists plowing contact between friction pairs (Ref 40, 41).

The wear rate of a Ni-20%Cr coating sliding against an Al₂O₃ counter material is displayed in Fig. 6 at 25 and 420 °C temperatures. At 420 °C, both samples show an increase in wear rate due to a mismatch in the thermal expansion rates of the coating and substrate. The difference causes increased adhesion and delamination wear. Notably, the reduced hardness of the Ni-20%Cr 3 Hz sample makes it more susceptible to high-temperature wear, resulting in a higher wear rate when compared to the Ni-20%Cr 6 Hz sample. The increased wear rates reported in nickel-based coatings may be due to material transfer from the coating to the counterpart (Ref 22, 28).

3.4 Post-wear Analysis

3.4.1 3D Profilometry of the Wear Tracks. Figure 7 and 8 displays the room and high temperature of 3D and 2D depth profiles of the worn-out surface of the wear track with loads of 5, 10, and 20 N. Before the wear test, the surface roughness (Ra) was $0.26 \pm 0.02 \mu\text{m}$ to maintain uniform surface conditions. Worn surface profiles like track width and depth are provided in Table 7. The wear volume is calculated from the depth and width of the wear tracks.

The 3 Hz coating exhibits a broader and more profound wear track than the 6 Hz coating in all loading and temperature conditions, as shown in Fig. 7, 8, and Table 7. It is likely due to the higher hardness, which better resists applied loads. The Archard wear model suggests that as the hardness of a material increases, its wear volume decreases, indicating that it can withstand more wear and tear during sliding contact (Ref 42). Due to the formation of oxide layers at 420 °C, the surface roughness value was $1.06 \pm 0.06 \mu\text{m}$. The coating experiences thermal softening, promoting more contact area, plastic deformation, and increased wear debris formation, resulting in material loss, indicating an increase in wear volume. Variations

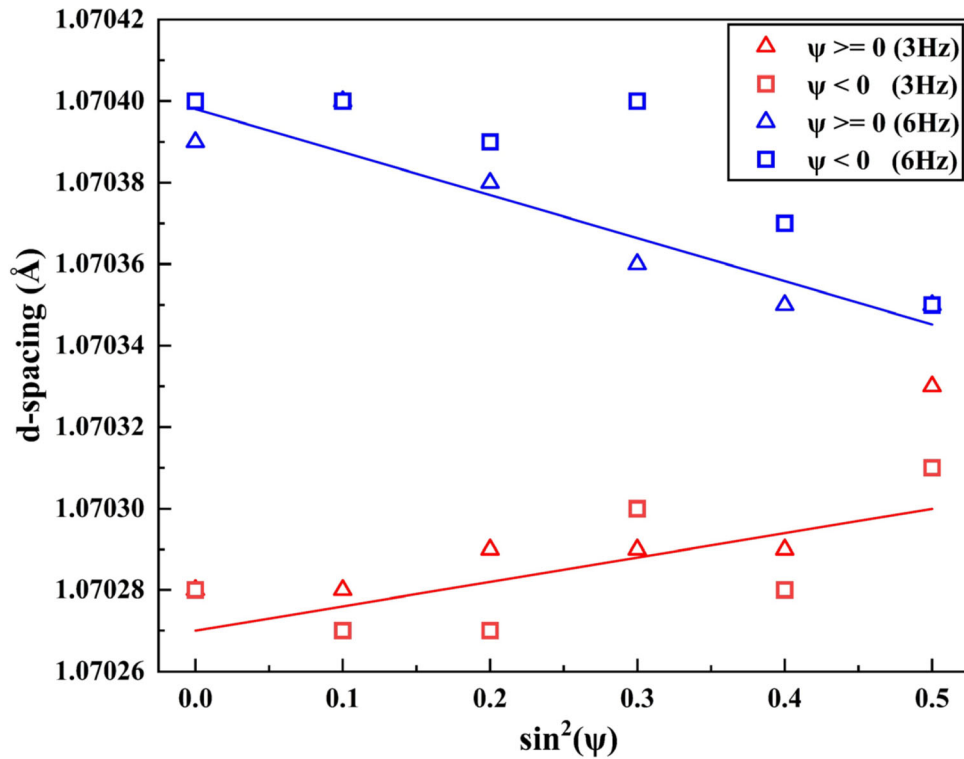


Fig. 4 Qualitative residual stress on both Ni-20%Cr coatings

Table 5 Vickers microhardness values with standard deviations

Coating	Spray frequency, Hz	Hardness (HV _{0.2})	
		25 °C	420 °C
Ni-20%Cr	3	348 ± 39	333 ± 23
	6	380 ± 40	366 ± 25

in detonation frequency during the deposition of Ni-20%Cr coatings affect adhesion and cohesion. Higher frequencies generally lead to stronger bonding between the coating and substrate, finer grain sizes, reduced porosity, and improved wear resistance and thermal stability.

3.4.2 Raman Spectroscopy Analysis of the Worn Surfaces. Figure 9 shows the Raman spectroscopy of coatings after the wear test at different temperatures and spray frequencies. At 25 °C, no noticeable oxide layers were seen on the worn surface of the wear track at normal wear processes. After wear tests at 420 °C, Raman spectra showed clear peaks associated with nickel oxide (NiO) at 546, 551, 904, and 1101 cm⁻¹ (Ref 43-45) and chromium oxide (Cr₂O₃) at 303, 305, 348, 662, and 691 cm⁻¹ (Ref 46, 47). However, the observed oxide peaks were relatively small, suggesting minor oxide particles instead of a thick, dominant oxide layer.

3.4.3 Evaluation of Wear Maps and Mechanisms. Figure 10 and 11 illustrates the wear maps of Ni-20%Cr coatings (3 and 6 Hz) at 25 and 420 °C under 5, 10, and 20 N loading conditions. FESEM wear maps of Ni-20%Cr coating show the ridges, grooves, microcracks, and crack propagation. These are

attributed to abrasive and surface fatigue wear mechanisms at room temperature caused by abrasive particles in the sliding contact area. Parallel furrows, grooves, and microplowing indicate abrasive wear. Microcracks on coating are induced during sliding wear tests due to residual stress (Ref 17). Continuous dry sliding, crack initiation, and propagation show the spread of microcracks (delamination), suggesting surface fatigue wear mechanisms (Ref 48).

Figure 11 reveals severe delamination, partial oxide particles, and partial oxide layers indicating adhesive, mild abrasive, and partial oxidative wear at high temperatures. The coating layers separated and experienced delamination and spalling due to thermal stresses and mechanical loads. Partial oxide formation was observed on the worn surface of the wear track and confirmed by Raman spectroscopy analysis. Wear rate depends on the extent of the wear mechanism, ranging from mild to severe. As hardness increases, wear rate decreases, and vice versa. High-temperature increases wear rate due to material transfer. At high temperatures, material hardness decreases, making it easier for loose abrasive particles to compact into rough layers, promoting a higher wear rate (Ref 49).

Despite the presence of oxide layers, the anticipated decrease in wear rate and reduction in CoF was not observed. Instead, the wear rate increased due to the formation of compact, small batches of powder oxide particles. The oxide layer acts as a self-lubricating property and reduces wear rate (Ref 23, 45). Still, suppose it is insufficient to resist the load. In that case, it breaks, leading to severe adhesive wear and the highest wear rate due to thermal softening and forming debris acting as abrasive particles. However, the wear rate increased due to the susceptibility to plastic flow at that temperature.

Table 6 Worn surface profiles of wear tracks at different conditions

Coating	Spray frequency, Hz	Loads, N	Width, μm		Depth, μm	
			25 °C	420 °C	25 °C	420 °C
Ni-20%Cr	3	5	387 ± 23	933 ± 70	5.6 ± 0.4	33.17 ± 1.7
		10	556 ± 11	1283 ± 76	12.4 ± 0.4	64.8 ± 4
		20	726 ± 20	1716 ± 35	20.5 ± 1.6	105 ± 3
	6	5	373 ± 5	700 ± 20	6.1 ± 0.5	33.2 ± 4
		10	490 ± 10	1266 ± 41	9.7 ± 0.1	54.7 ± 3.8
		20	580 ± 10	1586 ± 41	13.1 ± 0.4	93 ± 7

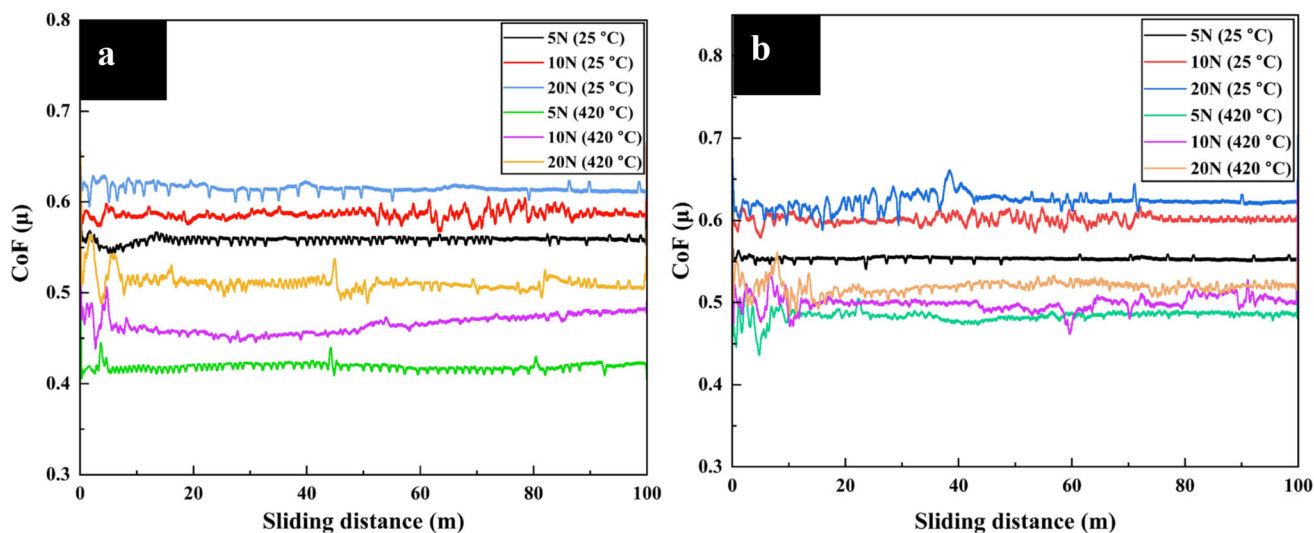


Fig. 5 CoF vs. sliding distance of Ni-20%Cr coating at 25 and 420 °C: (a) 3 Hz, (b) 6 Hz

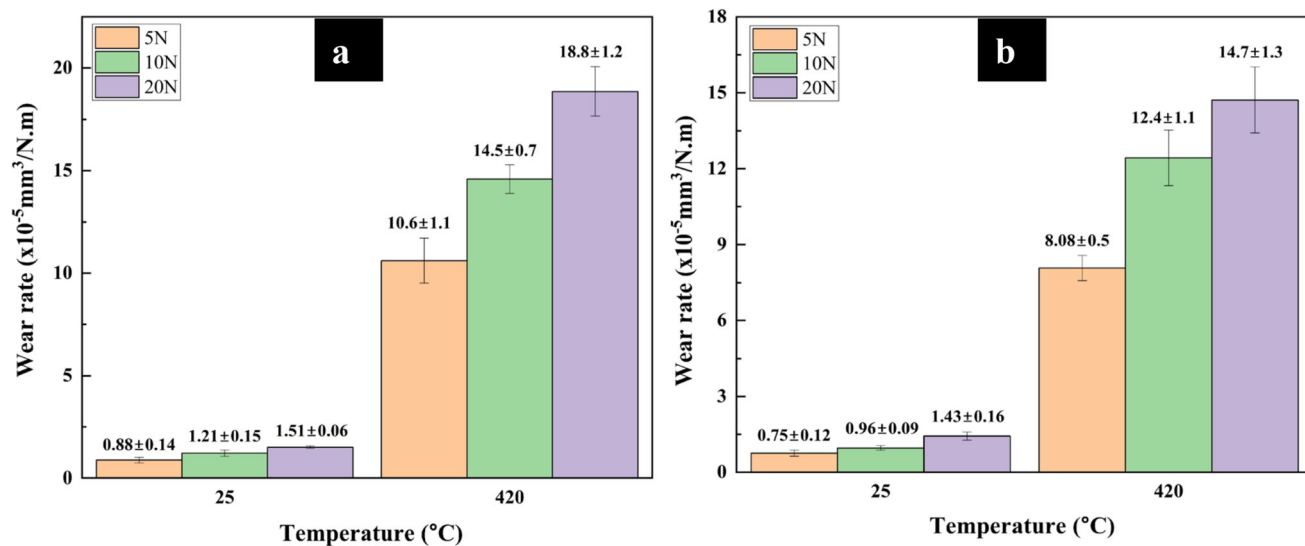


Fig. 6 Wear rate of coatings at different loads and temperatures. (a) 3 Hz and (b) 6 Hz

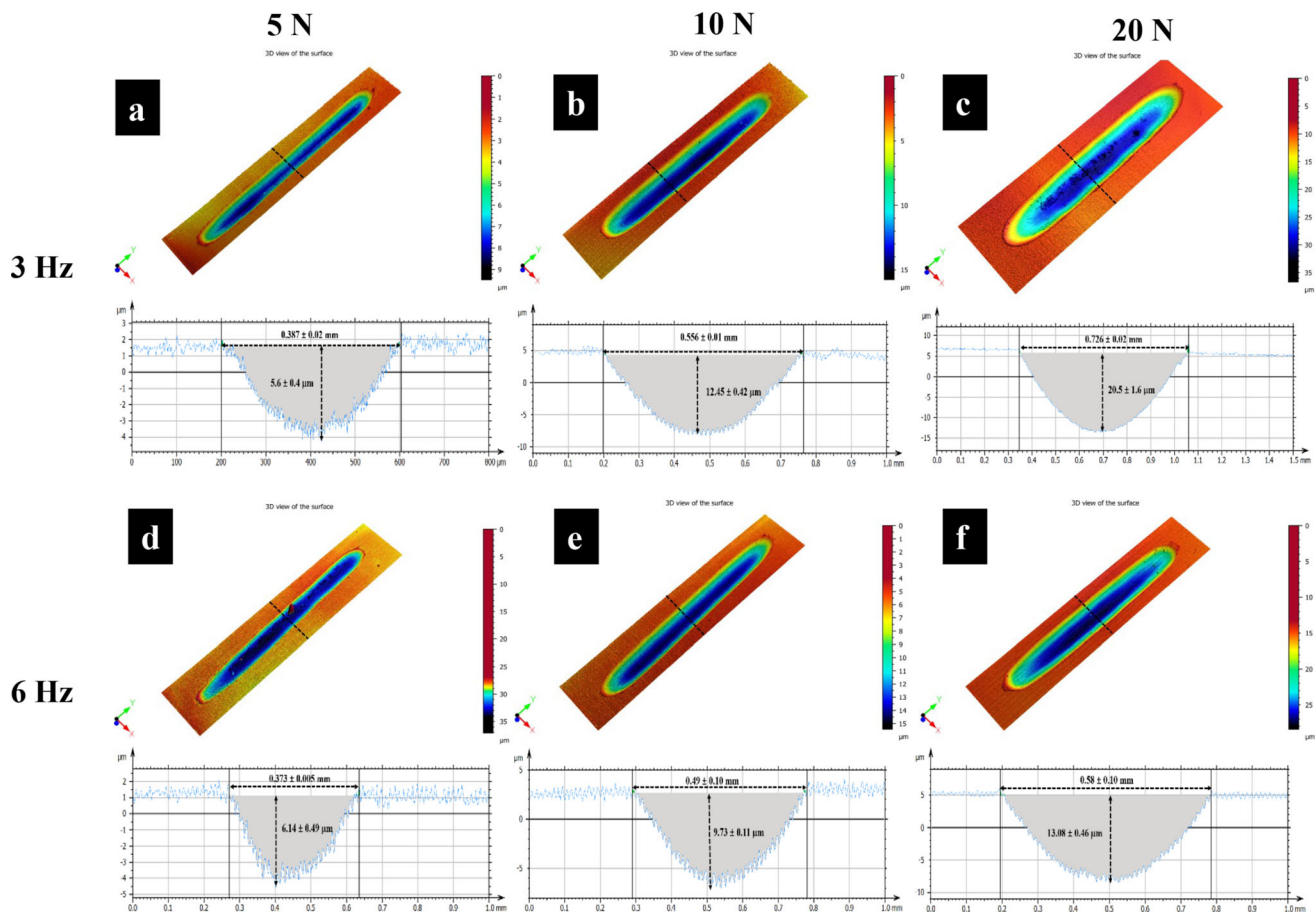


Fig. 7 Confocal 3D and 2D wear track profiles at 25 °C under different loads. (a, b, c) 3 Hz (d, e, f) 6 Hz

3.4.4 EDS Analysis of Wear Traces. FESEM-EDS analysis was conducted to determine the elemental composition at different temperatures. After the wear test, Fig. 12 shows the elemental mapping analysis of the wear track was almost equal to the as-sprayed coating composition. It indicates no oxide formation on the wear track at room temperature. At high temperatures (420 °C), EDS analysis (Fig. 13) shows an increase in oxygen percentage from 2-5% to 24%-26%. It confirmed the reaction with the coating composition to form the oxides, but the temperature did not produce a stable and dominant oxide layer. Table 7 displays the elemental composition of the wear track at elevated temperatures.

3.4.5 Analysis of Counter Material Used in the Wear Test. FESEM-EDS was used to analyze the alumina (Al_2O_3) ball employed as the counter material for the linear reciprocating wear test. The ball was smooth before the test, with significant wear experienced at ambient temperature (25 °C). Figure 14(a) displays the worn surface of counter material with deep abrasive grooves and ridges, indicating a complete abrasive wear mechanism. No microcracks were found on the

worn-out surface, suggesting surface fatigue did not contribute to the wear. EDS mapping analysis also confirmed no coating material transfer on the surface of the counter material.

At 420 °C, the worn surface of the alumina counter material showed apparent differences from the 25 °C. Figure 14(b) presents the material transfer and exchange, with delamination marks and adhesive wear debris from the coating material. The worn surface displayed numerous individual particles from the coatings spread out and gathered across it. However, at high temperatures, the presence of coating particles sticking on the worn surface of the wear scar and the wear mechanism was adhesive wear.

4. Conclusions

A study investigated detonation sprayed (DSC) Ni-20%Cr coatings at 3 and 6 Hz spray frequencies. The wear behavior was examined under dry sliding linear reciprocating conditions at 25 and 420 °C, and conclusions are below.

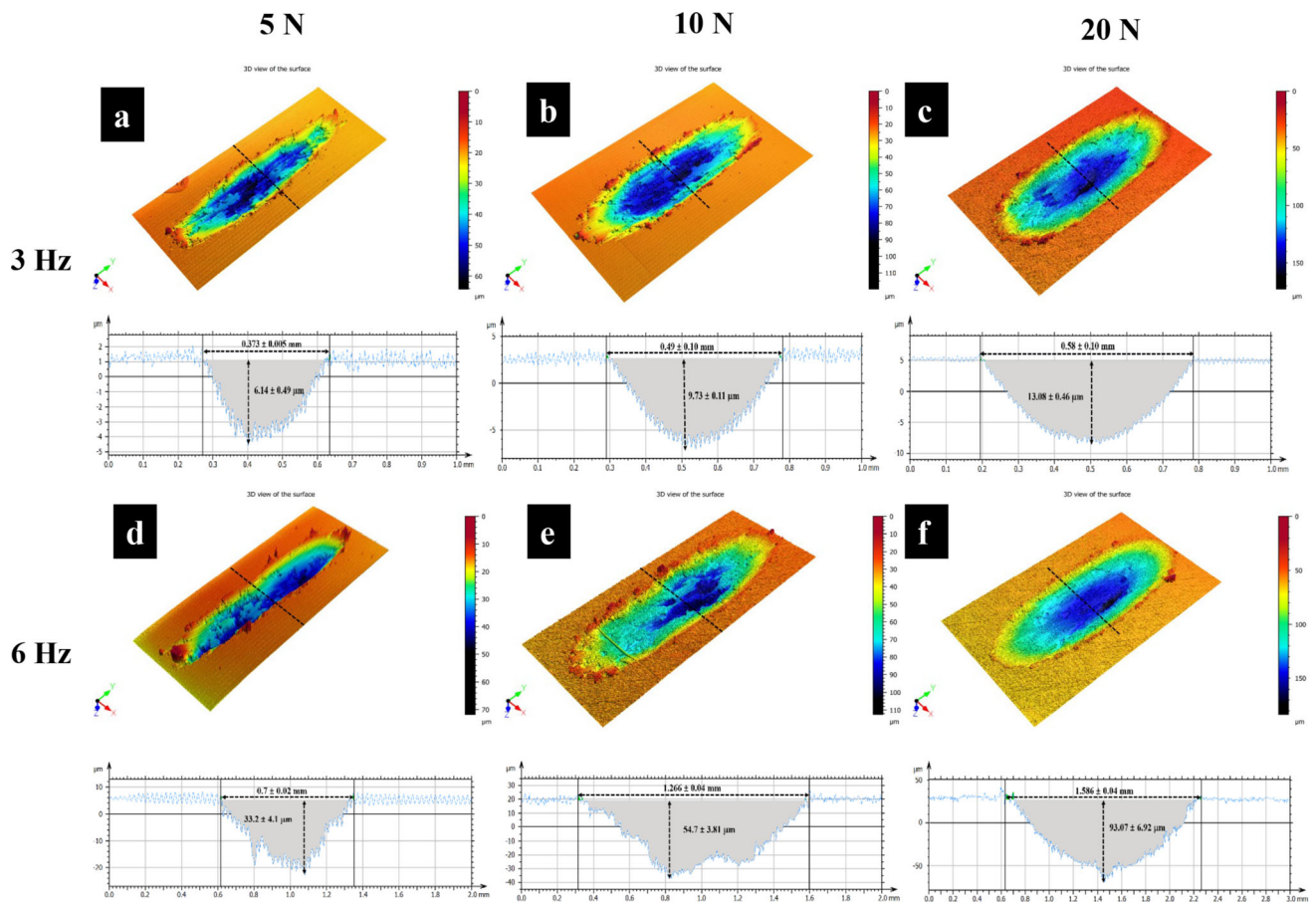


Fig. 8 Confocal 3D and 2D wear track profiles at 420 °C. (a, b, c) 3 Hz (d, e, f) 6 Hz

Table 7 EDS elemental mapping analysis of wear tracks at different temperatures

Coating	Spray frequency, Hz	Temperature, °C	Elemental composition, wt.%		
			Ni	Cr	O
Ni-20%Cr	3	25	73.9 ± 0.1	17.5 ± 0.3	6.7 ± 0.2
		420	70.3 ± 0.4	16.5 ± 0.2	12.1 ± 0.2
	6	25	74.5 ± 0.2	18.2 ± 0.1	6.8 ± 0.1
		420	69.8 ± 0.4	15.8 ± 0.3	12.9 ± 0.5

1. The Ni-20%Cr coating shows a uniform microstructure with melted, partially oxidized, and metallic particles. 6 Hz showed higher thickness and hardness than 3 Hz due to enhanced bonding and deformation of splats, resulting in superior mechanical properties.
2. The Ni-20%Cr 6 Hz coating showed compressive residual stress, while the Ni-20%Cr 3 Hz coating had tensile residual stress. This difference was due to the higher peening effect, thickness, and hardness, causing a transition from tensile to compressive residual stress.
3. The friction coefficient reduces at 420 °C due to thermal softening and inadequate oxide layer formation, but the wear rate increases with loads due to abrasive loss and surface roughness. Ni-20%Cr 6 Hz has a lower wear rate due to higher hardness.
4. The wear mechanism at 25 °C is mainly abrasion, surface fatigue, and mild adhesion, while at 420 °C, it becomes more severe and complex, involving adhesive wear and partial oxidation.

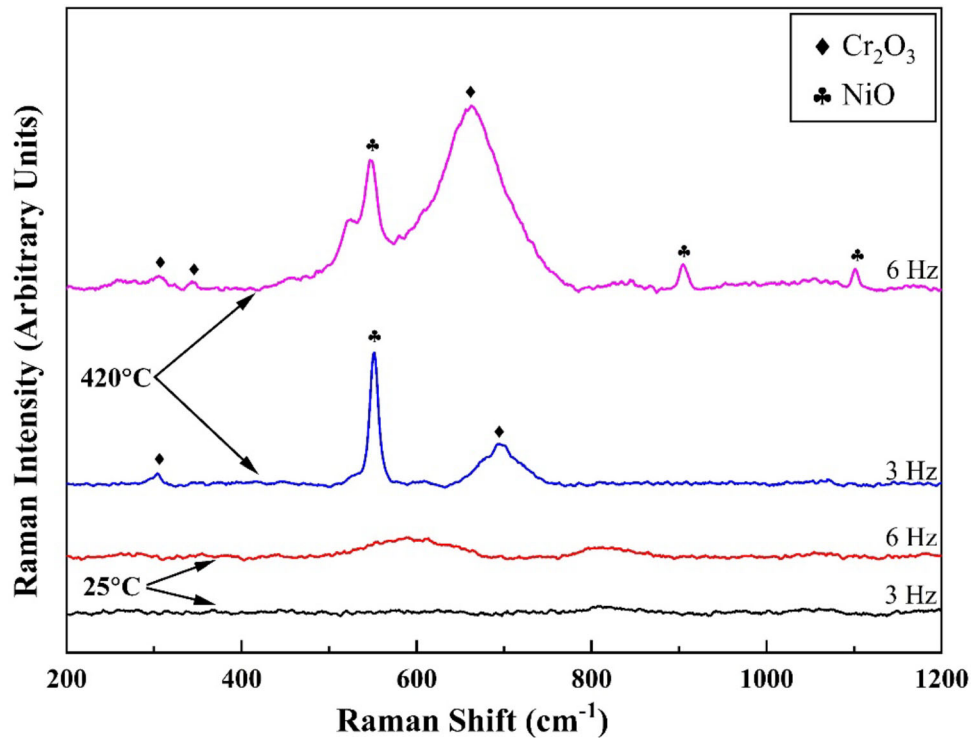


Fig. 9 Raman peaks of 3 and 6 Hz coating at 25 and 420 °C

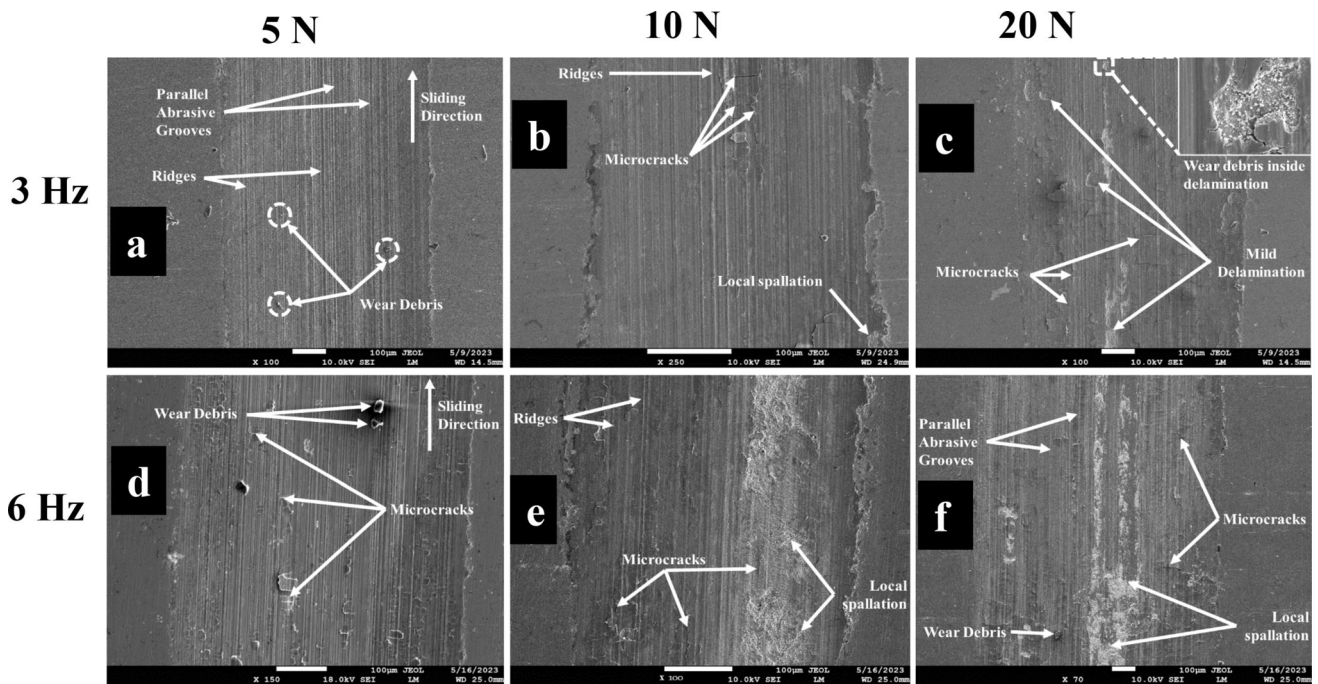


Fig. 10 Worn surface of wear track at room temperature under different loads. (a–c) 3 Hz, (d–f) 6 Hz

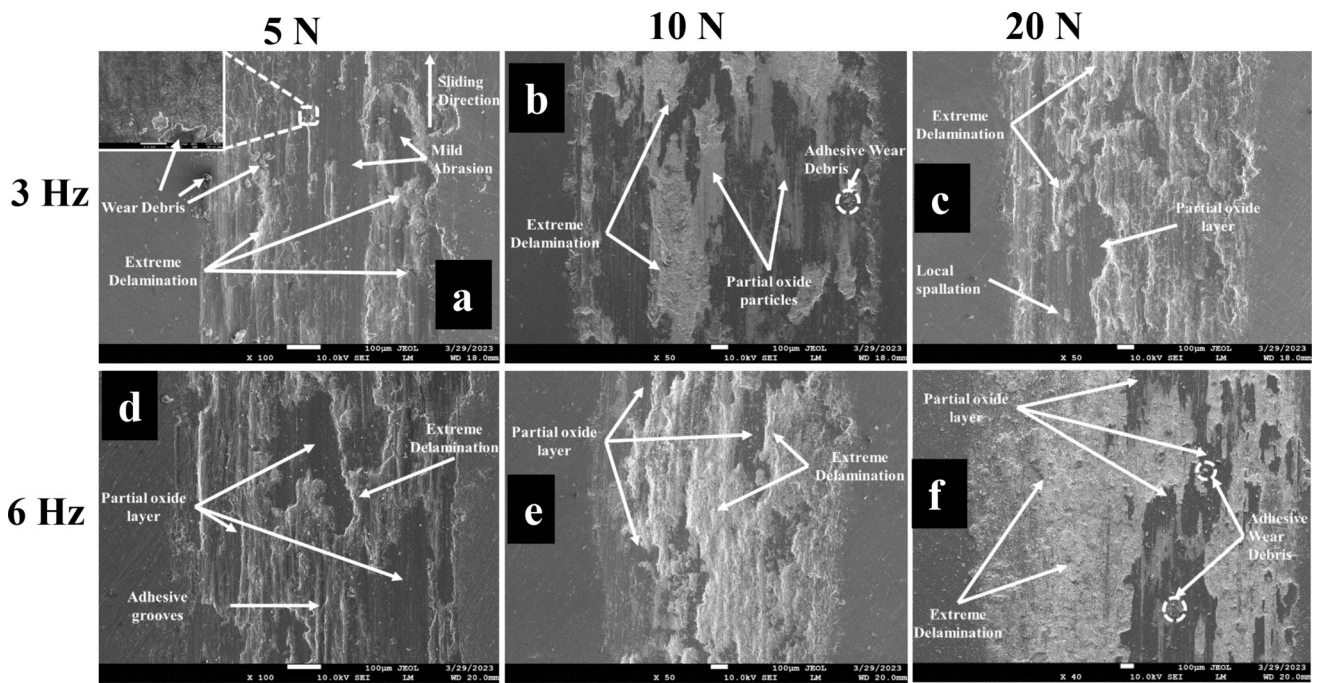


Fig. 11 Worn surface of wear tracks at high temperatures under various loads. (a–c) 3 Hz, (d–f) 6 Hz

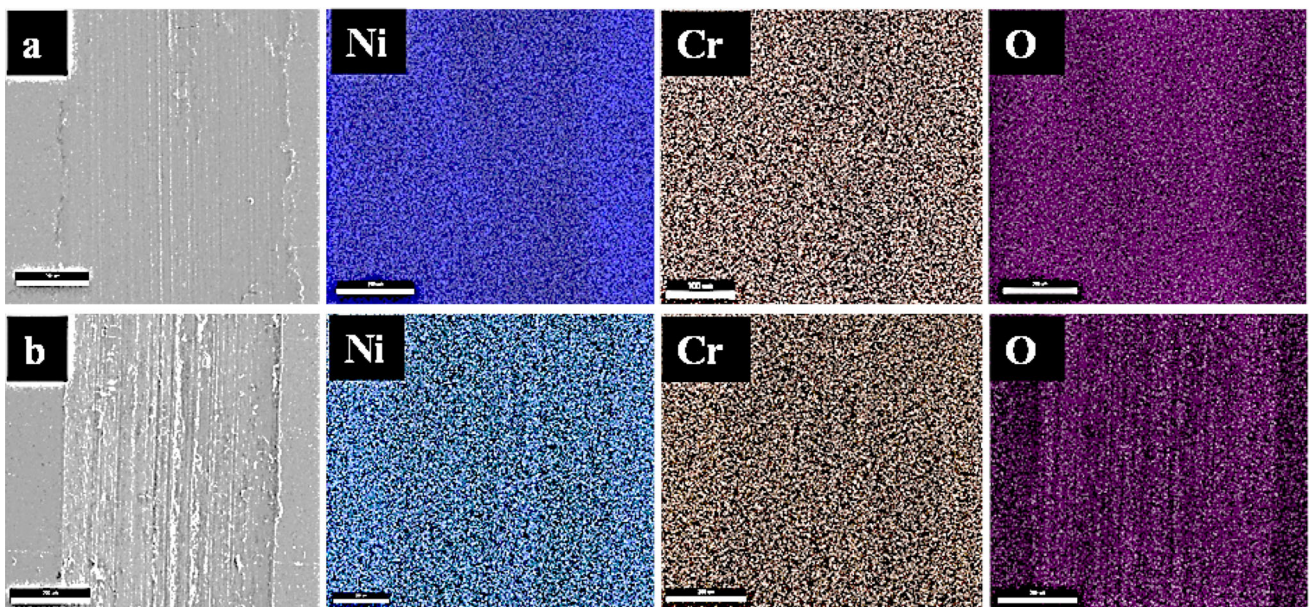


Fig. 12 Elemental mapping analysis of worn surface at 25 °C. (a) 3 Hz and (b) 6 Hz

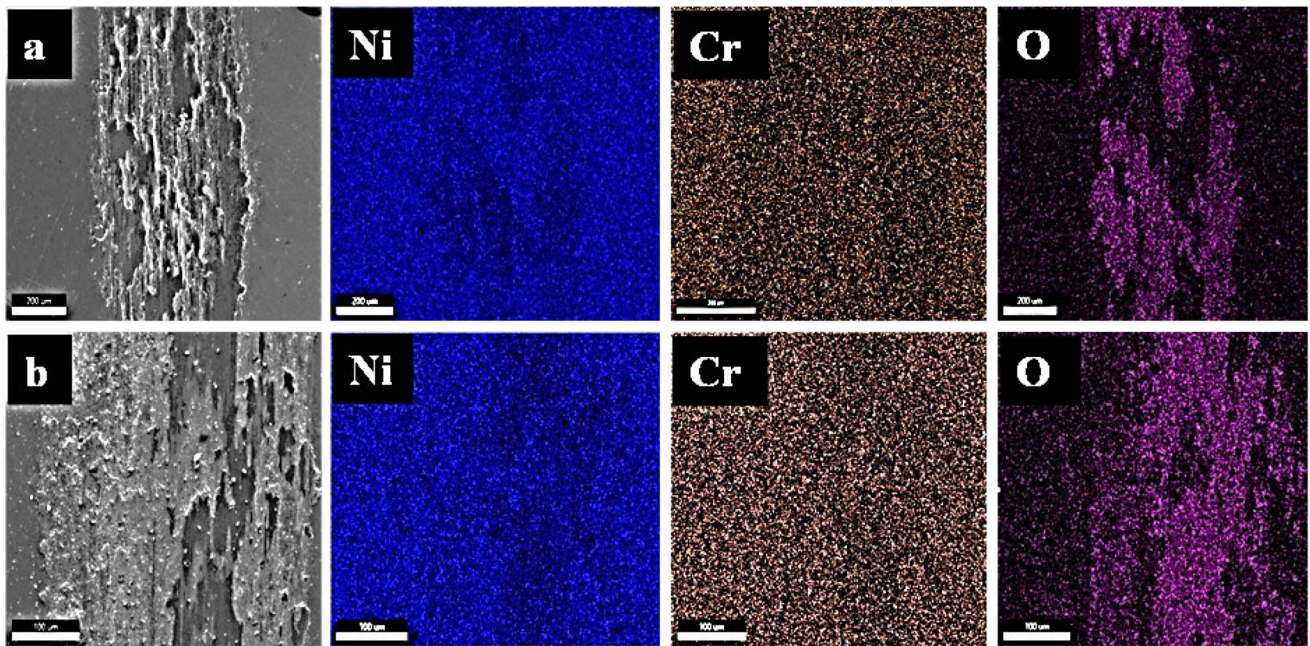


Fig. 13 Elemental mapping analysis of worn surface at 420 °C. (a) 3 Hz and (b) 6 Hz

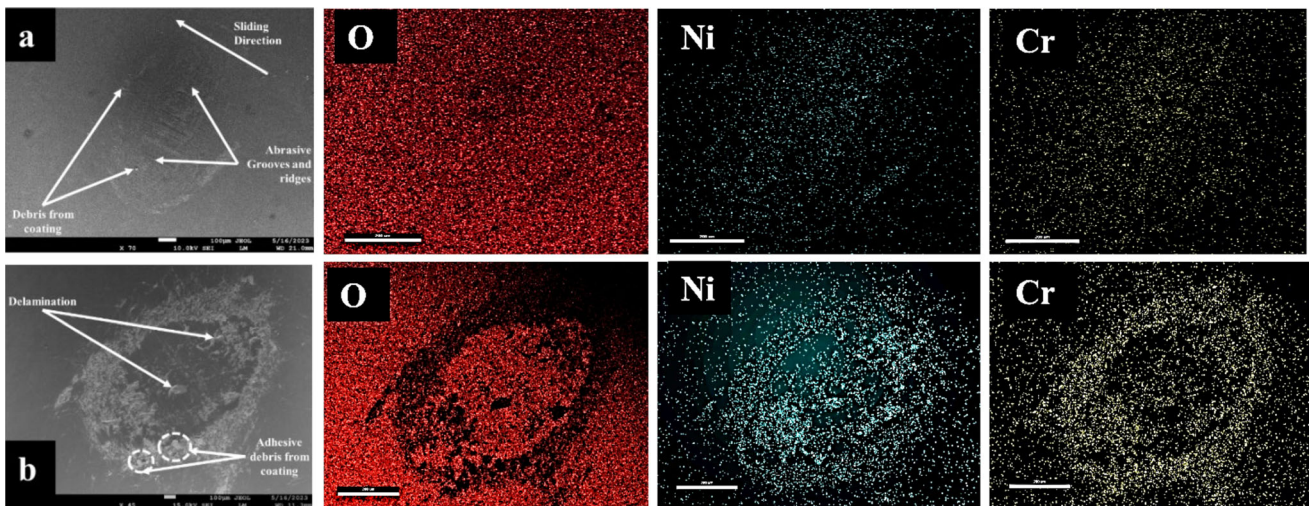


Fig. 14 Micrographs and EDS analysis of alumina ball. (a) 25 °C and (b) 420 °C

References

1. A. Nowotnik, Nickel-Based Superalloys, *Ref. Module Mater. Sci. Mater. Eng.*, 2016 <https://doi.org/10.1016/B978-0-12-803581-8.02574-1>
2. W. Grzesik, P. Niesłony, W. Habrat, J. Sieniawski and P. Laskowski, Investigation of Tool Wear in the Turning of Inconel 718 Superalloy in Terms of Process Performance and Productivity Enhancement, *Tribol. Int.*, 2018, **118**, p 337–346
3. T. Rong and D. Gu, Formation of Novel Graded Interface and Its Function on Mechanical Properties of WC1-x Reinforced Inconel 718 Composites Processed by Selective Laser Melting, *J. Alloys Compd.*, 2016, **680**, p 333–342
4. S. Saladi, J. Menghani and S. Prakash, A Study on the Cyclic Oxidation Behavior of Detonation-Gun-Sprayed Ni-5Al Coatings on Inconel-718 at 900 °C, *J. Mater. Eng. Perform.*, 2014, **23**(12), p 4394–4403. <https://doi.org/10.1007/S11665-014-1240-0/FIGURES/8>
5. S.B. Mishra, K. Chandra and S. Prakash, Dry Sliding Wear Behaviour of Nickel-, Iron- and Cobalt-Based Superalloys, *Tribol. Mater. Surf. Interfaces*, 2013, **7**(3), p 122–128. <https://doi.org/10.1179/1751584X13Y.0000000038>
6. K. Holmberg and A. Erdemir, Influence of Tribology on Global Energy Consumption Costs and Emissions, *Friction*, 2017, **5**(3), p 263–284. <https://doi.org/10.1007/S40544-017-0183-5/METRICS>
7. N. Purushotham, B. Rajasekaran, N.L. Parthasarathi, K. Praveen and G. Sivakumar, Sliding Wear Behaviour of Ni-5 %Al Coating Deposited by Detonation Spray on IN718, *Mater. Today Proc.*, 2022, **65**, p 3741–3747. <https://doi.org/10.1016/j.matpr.2022.06.425>
8. E. Hao, X. Zhao, Y. An, W. Deng, H. Zhou and J. Chen, The Effect of Pre-Oxidation on Microstructure, Mechanical Properties and High-Temperature Tribological Behaviors of HVOF-Sprayed NiCoCrAlYTa Coating, *Appl. Surf. Sci.*, 2019, **489**, p 187–197. <https://doi.org/10.1016/j.apsusc.2019.05.334>
9. N. Chavana and V. Bhajantri F, and S.C. Jambagi, Improvement in Slurry Erosion and Corrosion Resistance of Plasma-Sprayed Fly Ash Coatings for Marine Applications, *ACS Omega*, 2022 <https://doi.org/10.1021/acsomega.2c03800>
10. C. Sundaresan, B. Rajasekaran, S. Varalakshmi, K. Santhy, D.S. Rao and G. Sivakumar, Comparative Hot Corrosion Performance of APS

- and Detonation Sprayed CoCrAlY, NiCoCrAlY and NiCr Coatings on T91 Boiler Steel, *Corros. Sci.*, 2021, **189**, p 109556
11. V. Kala, K. Santhy, G. Sivakumar and B. Rajasekaran, Understanding the Initial Stage Oxidation and Microstructural Evolution of Detonation Sprayed NiCoCrAlY Bond Coat Using In-Situ High-Temperature X-Ray Diffraction, *Corros. Sci.*, 2022, **207**, p 110521
 12. N. Purushotham, K. Santhy, P. Suresh Babu, G. Sivakumar and B. Rajasekaran, In Situ High-Temperature X-Ray Diffraction Study on Atmospheric Plasma and Detonation Sprayed Ni-5 Wt.%Al Coatings, *J. Therm. Spray Technol.*, 2023 <https://doi.org/10.1007/s11666-023-01627-w>
 13. D. Lubell, C. DellaCorte, and M. Stanford, "Test Evolution and Oil-Free Engine Experience of a High Temperature Foil Air Bearing Coating," *Proceedings of the ASME Turbo Expo*, American Society of Mechanical Engineers Digital Collection, 2006, p 1245–1249, <https://doi.org/10.1115/GT2006-90572>
 14. K. Radil and C. DellaCorte, The Performance of PS400 Subjected to Sliding Contact at Temperatures from 260 to 927 C, *Taylor Fr.*, 2017, **60**(6), p 957–964. <https://doi.org/10.1080/10402004.2016.1231357>
 15. B. Li, Y. Gao, X. Hou, C. Li, H. Guo, Y. Kang, Y. Li, Q. Zheng and S. Zhao, Microstructure, Mechanical and Tribological Properties of NiAl Matrix Composites with Addition of BaO/TiO₂ Binary Oxides, *Tribol. Int.*, 2020, **144**, p 106108
 16. P. Shi, S. Wan, G. Yi, H. Sun, Y. Yu, E. Xie, Q. Wang, S.Z. Shen and N. Alam, TiO₂-ZnO/Ni-5wt.%Al Composite Coatings on GH4169 Superalloys by Atmospheric Plasma Spray Techniques and Their Elevated-Temperature Tribological Behavior, *Ceram. Int.*, 2020, **46**(9), p 13527–13538. <https://doi.org/10.1016/j.ceramint.2020.02.138>
 17. X. Wang, X. Feng, C. Lu, G. Yi, J. Jia and H. Li, Mechanical and Tribological Properties of Plasma Sprayed NiAl Composite Coatings with Addition of Nanostructured TiO₂/Bi₂O₃, *Surf. Coatings Technol.*, 2018, **349**, p 157–165
 18. M.B. Peterson, S.J. Calabrese, S.Z. Li and X.X. Jiang, Paper I (II) Frictional Properties of Lubricating Oxide Coatings, *Tribol. Ser.*, 1990, **17**(C), p 15–25
 19. H. Kato and K. Komai, Tribofilm Formation and Mild Wear by Tribo-Sintering of Nanometer-Sized Oxide Particles on Rubbing Steel Surfaces, *Wear*, 2007, **262**(1–2), p 36–41
 20. S.M. Aouadi, H. Gao, A. Martini, T.W. Scharf and C. Muratore, Lubricious Oxide Coatings for Extreme Temperature Applications: A Review, *Surf. Coat. Technol.*, 2014, **257**, p 266–277
 21. S. Hernandez, J. Hardell, H. Winkelmann, M.R. Ripoll and B. Prakash, Influence of Temperature on Abrasive Wear of Boron Steel and Hot Forming Tool Steels, *Wear*, 2015, **338–339**, p 27–35
 22. G. Bolelli, C. Vorkötter, L. Lusvardi, S. Morelli, V. Testa and R. Vaßen, Performance of Wear Resistant MCrAlY Coatings with Oxide Dispersion Strengthening, *Wear*, 2020, **444–445**, 203116
 23. N. Purushotham, N.L. Parthasarathi, P.S. Babu, G. Sivakumar and B. Rajasekaran, Effect of Thermal Expansion on the High Temperature Wear Resistance of Ni-20%Cr Detonation Spray Coating on IN718 Substrate, *Surf. Coat. Technol.*, 2023 <https://doi.org/10.1016/J.SURF.COAT.2023.129490>
 24. J.J. Ayerdi, A. Aginagalde, I. Llavori, J. Bonse, D. Spaltmann and A. Zabala, Ball-on-Flat Linear Reciprocating Tests: Critical Assessment of Wear Volume Determination Methods and Suggested Improvements for ASTM D7755 Standard, *Wear*, 2021, **470–471**, 203620
 25. S. Sharma, S. Sangal and K. Mondal, Influence of Subsurface Structure on the Linear Reciprocating Sliding Wear Behavior of Steels with Different Microstructures, *Metall. Mater. Trans. A Phys. Metall. Mater. Sci.*, 2014, **45**(13), p 6088–6102. <https://doi.org/10.1007/S11661-014-2555-Z/FIGURES/13>
 26. R. Ahmed and M. Hadfield, Experimental Measurement of the Residual Stress Field within Thermally Sprayed Rolling Elements, *Wear*, 1997, **209**(1–2), p 84–95
 27. P. Bansal, P.H. Shipway and S.B. Leen, Residual Stresses in High-Velocity Oxy-Fuel Thermally Sprayed Coatings – Modelling the Effect of Particle Velocity and Temperature during the Spraying Process, *Acta Mater.*, 2007, **55**(15), p 5089–5101
 28. M. Kiryc, D. Kurumlu, G. Eggeler, R. Vaßen and G. Marginean, On the Sliding Wear and Solid Particle Erosion Behaviour of HVOF-Sprayed CoNiCrAlY Coatings and NiCrCoTi Substrates in Dependence of the Oxidation Dwell Time at 900 °C, *Surf. Coatings Technol.*, 2023, **453**, p 129137
 29. P. Saravanan, V. Selvarajan, S.V. Joshi and G. Sundararajan, Experimental Design and Performance Analysis of Alumina Coatings by a Detonation Spray Process, *J. Phys. D Appl. Phys.*, 2001, **34**(1), p 131. <https://doi.org/10.1088/0022-3727/34/1/320>
 30. L. Singh, V. Chawla and J.S. Grewal, A Review on Detonation Gun Sprayed Coatings, *J. Miner. Mater. Charact. Eng.*, 2012, **11**(03), p 243–265. <https://doi.org/10.4236/jmmce.2012.113019>
 31. M. Samodurova, N. Shaburova, O. Samoilo, A.O. Moghaddam, K. Pashkev, V. Ulyanitskiy and E. Trofimov, Properties of WC–10%Co–4%Cr Detonation Spray Coating Deposited on the Al–4%Cu–1%Mg Alloy, *Materials (Basel)*, 2021, **14**(5), p 1206. <https://doi.org/10.3390/ma14051206>
 32. T.G. Wang, S.S. Zhao, W.G. Hua, J.B. Li, J. Gong and C. Sun, Estimation of Residual Stress and Its Effects on the Mechanical Properties of Detonation Gun Sprayed WC–Co Coatings, *Mater. Sci. Eng. A*, 2010, **527**(3), p 454–461
 33. Y.Y. Santana, P.O. Renault, M. Sebastiani, J.G. La Barbera, J. Lesage, E. Bemporad, E. Le Bourhis, E.S. Puchi-Cabrera and M.H. Staia, Characterization and Residual Stresses of WC–Co Thermally Sprayed Coatings, *Surf. Coatings Technol.*, 2008, **202**(18), p 4560–4565
 34. Y. Yarali Ozbek, C. Sarioglu and M. Durman, The Effect of Plasma Detonation Parameters on Residual Stresses Developed in the Plasma Modified Layer, *Vacuum*, 2014, **106**, p 11–15
 35. R. Gadow, M.J. Riegert-Escribano and M. Buchmann, Residual Stress Analysis in Thermally Sprayed Layer Composites, Using the Hole Milling and Drilling Method, *J. Therm. Spray Technol.*, 2005, **14**(1), p 100–108. <https://doi.org/10.1361/10599630522756/METRICS>
 36. Y. Bai, Z.H. Han, H.Q. Li, C. Xu, Y.L. Xu, Z. Wang, C.H. Ding and J.F. Yang, High Performance Nanostructured ZrO₂ Based Thermal Barrier Coatings Deposited by High Efficiency Supersonic Plasma Spraying, *Appl. Surf. Sci.*, 2011, **257**(16), p 7210–7216
 37. C.H. Hager, J. Sanders, S. Sharma, A. Voevodin and A. Segall, The Effect of Temperature on Gross Slip Fretting Wear of Cold-Sprayed Nickel Coatings on Ti6Al4V Interfaces, *Tribol. Int.*, 2009, **42**(3), p 491–502
 38. D.M. Nuruzzaman and M.A. Chowdhury, Effect of Normal Load and Sliding Velocity on Friction Coefficient of Aluminum Sliding Against Different Pin Materials, *Am. J. Mater. Sci.*, 2012, **2012**(1), p 26–31. <https://doi.org/10.5923/j.materials.2012020105>
 39. S.R. Pearson, P.H. Shipway, J.O. Abere and R.A.A. Hewitt, The Effect of Temperature on Wear and Friction of a High Strength Steel in Fretting, *Wear*, 2013, **303**(1–2), p 622–631
 40. F. Ye, Z. Lou, Y. Wang and W. Liu, Wear Mechanism of Ag as Solid Lubricant for Wide Range Temperature Application in Micro-Beam Plasma Cladded Ni60 Coatings, *Tribol. Int.*, 2022, **167**, p 107402
 41. W. Li, C. Huang, M. Yu, D. Liu, Y. Feng and H. Liao, Investigation of High Temperature Oxidation Behavior and Tribological Performance on Cold Sprayed Nickel-Alumina Composite Coating, *Surf. Coat. Technol.*, 2014, **239**(95), p 101
 42. J.F. Archard, Contact and Rubbing of Flat Surfaces, *J. Appl. Phys.*, 1953, **24**(8), p 981–988. <https://doi.org/10.1063/1.1721448>
 43. B.T. Sone, X.G. Fuku and M. Maaza, Physical & Electrochemical Properties of Green Synthesized Buzenite NiO Nanoparticles via Extracts, *Int. J. Electrochem. Sci.*, 2016, **11**(10), p 8204–8220. <https://doi.org/10.20964/2016.10.17>
 44. M.P. Kumar, G. Murugadoss and M.R. Kumar, Synthesis and Characterization of CuO–NiO Nanocomposite: Highly Active Electrocatalyst for Oxygen Evolution Reaction Application, *J. Mater. Sci. Mater. Electron.*, 2020, **31**(14), p 11286–11294. <https://doi.org/10.1007/s10854-020-03677-0>
 45. N. Purushotham, N.L. Parthasarathi, P. Suresh Babu, G. Sivakumar and B. Rajasekaran, High Temperature Sliding Wear Behavior of Detonation Sprayed Ni-5wt % Al Coating, *Wear*, 2023, **530–531**(February), p 205030. <https://doi.org/10.1016/j.wear.2023.205030>
 46. M. Mohammadtaheri, Q. Yang, Y. Li and J. Corona-Gomez, The Effect of Deposition Parameters on the Structure and Mechanical Properties of Chromium Oxide Coatings Deposited by Reactive Magnetron Sputtering, *Coatings*, 2018, **8**(3), p 111. <https://doi.org/10.3390/coating8030111>
 47. A.S.O. Gomes, N. Yaghini, A. Martinelli and E. Ahlberg, A Micro-Raman Spectroscopic Study of Cr(OH)₃ and Cr₂O₃ Nanoparticles Obtained by the Hydrothermal Method, *J. Raman Spectrosc.*, 2017, **48**(10), p 1256–1263. <https://doi.org/10.1002/jrs.5198>

48. A. Fischer, W. Dudzinski, B. Gleising and P. Stemmer, *Analyzing Mild- and Ultra-Mild Sliding Wear of Metallic Materials by Transmission Electron Microscopy*, Springer, Cham, 2018, p 29–59. https://doi.org/10.1007/978-3-319-99897-8_2
49. P. Shi, W. Wang, S. Wan, Q. Gao, H. Sun, X. Feng, G. Yi, E. Xie and Q. Wang, Tribological Performance and High Temperature Oxidation Behaviour of Thermal Sprayed Ni- and NiCrAlY-Based Composite Coatings, *Surf. Coatings Technol.*, 2021, **405**, p 126615

Publisher's Note Springer Nature remains neutral with regard to jurisdictional claims in published maps and institutional affiliations.

Springer Nature or its licensor (e.g. a society or other partner) holds exclusive rights to this article under a publishing agreement with the author(s) or other rightsholder(s); author self-archiving of the accepted manuscript version of this article is solely governed by the terms of such publishing agreement and applicable law.